Leadership in Sustainable Infrastructure

Leadership en Infrastructures Durables

Vancouver, Canada

May 31 – June 3, 2017/ *Mai 31 – Juin 3, 2017*

INFLUENCE OF Ti2Ni PRECIPITATES ON PHASE TRANSFORMATION AND MECHANICAL PROPERTY OF Ni-Ti-Fe SHAPE MEMORY ALLOY

Yulong Liang [1], Shuyong Jiang [2,4], M.Shahria Alam[3] and Yanqiu Zhang [2]
[1] College of Mechanical and Electrical Engineering, Harbin Engineering University, Harbin, 150001, China
[2] College of Materials Science and Chemical Engineering, Harbin Engineering University, Harbin, 150001, China
[3] School of Engineering, The University of British Columbia, Kelowna, BC, Canada V1V1V7
[4] jiangshy@sina.com

Abstract Three novel shape memory alloys (SMAs), $Ti_{51.8}Ni_{(45-x)}Fe_{3.2}Si_x$ (x=0.3, 0.6, 0.9 ; at.%), were designed in order to investigate the influence of Ti_2Ni precipitates on the phase transformation and mechanical properties of Ni-Ti-Fe-Si alloys. By adding a small amount of silicon and increasing the content of titanium, plenty of Ti_2Ni precipitates will generate in the Ni-Ti-Fe-Si alloys. The addition of varying contents of silicon has a great influence on the size and shape of Ti_2Ni precipitates. As a hard and brittle precipitate, the Ti_2Ni precipitates, which have different sizes and morphologies and were surrounded by strain fields, can affect the phase transformation behavior and mechanical properties of Ni-Ti-Fe SMAs. Results show that the phase transformation behavior of three kinds of Ni-Ti-Fe-Si alloys is almost same, while the transformation temperature exhibits a slight variation by changing the size and morphology of Ti_2Ni. Findings also revealed that the rupture strength of $Ti_{51.8}Ni_{44.4}Fe_{3.2}Si_{0.6}$ can reach 1550 MPa due to the presence of small Ti_2Ni particles. By comparing $Ti_{51.8}Ni_{44.1}Fe_{3.2}Si_{0.9}$ and $Ti_{51.8}Ni_{44.7}Fe_{3.2}Si_{0.3}$, it was observed that the yield strength can be improved at a certain size of Ti_2Ni precipitates.

1 INTRODUCTION

As we all know, Nickel-titanium shape memory alloys(NiTi) are widely used in mechanical, aerospace, medical and biological industries for its plentiful phase transformation behaviors, good mechanical properties, high biocompatibility excellent shape memory effect(SME) and superelasticity. In recent years, a variety of Ni-Ti based shape memory alloys have been developed and used in many engineering applications due to their various transformation temperature as well as some mechanical properties. It is well known that the properties of TiNi-based alloys are extremely sensitive to original chemical composition as well as the subsequent processings(Wang, Liu, and Cao 2010; Mehrabi et al. 2008). A large amount of attempts have focused on the effect of third or fourth alloying elements on the transformation behaviors and mechanical properties. The addition of a third element to the basic composition is able to change NiTi SMA's many properties. For example, adding Nb to NiTi SMA can significantly increase the temperature hysteresis of the phase transformations (As-Ms, As~austenite transformation start temperature, Ms~martensite transformation start temperature) to 150 K(Zhang et al. 1991), while the addition of Fe will greatly decrease the Ms temperature(Marquina et al. 1994).

At present, the SMAs used as couplings in aircraft are mainly Ni-Ti-Nb and Ni-Ti-Fe SMAs. Ni-Ti-Nb SMA couplings with a wide temperatures hysteresis of phase transformation can be stored at room temperature after martensite deformation at a low temperature. However, stress-induced martensite phase transformation happened at low temperature in the Ni-Ti-Nb SMAs leading to the failure of couplings. Compared with Ni-Ti-Nb, Ni-Ti-Fe SMA has a lower Ms, which overcomes the shortcomings of stress-induced martensite phase transformation at low temperature. It was reported that Ni-Ti-Fe based SMA couplings ($Ms \leq 223K$) in which Fe substitutes for Ni were first used in the engineering application due to its low Ms temperature and good high-temperature stability(Qian et al. 2006). The addition of Fe element not only greatly decrease the transformation temperature of martensite，but the two-stage phase transformations from high-temperature parent phase with a B2 structure to an intermediate (R) phase with a rhombohedral structure and then to low-temperature martensite phase with a monoclinic B19′ structure, could also be observed clearly without another special treatment(Salamon, Meichle, and Wayman 1985). So Ni-Ti-Fe SMA have become a hot research topic in the field of SMA. The current researches about NiTiFe are mainly focused on the R-phase transformation behaviors(Basu et al. 2015) and the influence of adding rare earth on thermomechanical properties(Wang, Liu, and Cao 2010). It has been reported that in equi-atomic or slightly Ti-rich NiTi alloys, Ti_2Ni phase forms during solidification of the alloy from the melt(Wu and Wu 2010; Kim and Jang 2013; Gao and Wang 2008). Meanwhile, Si is a beneficial element for SMA, and the addition of Si will make the austenite solid solution strengthening, lower the néel temperature(Sato et al. 1984) and stacking fault energy in austenite(Gallagher 1970). According to the literature(Nagarajan and Chattopadhyay 1994), the addition of Si to Ni-Ti based alloys stabilizes icosahedral clusters and the clusters can subsequently serve as embryos for Ti_2Ni. Also the volume fraction of Ti_2Ni increases with increase in the Ti content of the alloy. Because of Fe substituting Ni in Ni-Ti-Fe alloys, the content of Ti is generally higher than Ni in Ni-Ti-Fe alloys. The Ti_2Ni phase is likely to form in Ni-Ti-Fe alloys and however, studies about the effects of Ti_2Ni on transition and mechanical behavior in NiTiFe alloys has been scarce to our knowledge.

In this work, we have processed the composition $Ti_{51.8}Ni_{(45-x)}Fe_{3.2}Si_x$ (x=0.3, 0.6, 0.9；at.%), with the purpose of figuring out the influence of Ti_2Ni precipitates on phase transformation behaviors and mechanical properties in Ti-Ni-Fe-Si alloys with different Si content.

2 EXPERIMENTS

The alloys $Ti_{51.8}Ni_{(45-x)}Fe_{3.2}Si_x$ (x=0.3, 0.6, 0.9；at.%) were produced in 50g batches by combining high pure elements (Ti sheets, Ti>99.4% wt%; Ni plates, Ni>99.98% wt%; Fe slices, Fe>99.7% wt%; Si blocks, Si>99.999%) in stoichiometric amounts and vacuum arc melting using a copper crucible. The as-melted buttons were sealed in evacuated quartz tubes and went through a further homogenizing treatment at 1000℃ for 24 h followed by quenching into ice water without seal broken. Subsequently, all specimens for the following experiments were cutting out from the buttons by means of wire electrical discharge machining(WEDM).

The Ni-Ti-Fe-Si specimens for optical microscopy were prepared by mechanical polishing method and etched in $HF\text{-}HNO_3\text{-}H_2O$ solution in a volume ratio of 1:6:7 for approximately 10s. The microstructures and phase chemical compositions were characterized by FEI-QUANTA-200 scanning electron microscope(SEM) equipped with energy dispersive spectroscopy(EDS) analysis system. In order to identify the crystal structures and phase composition of the polycrystalline alloys, the X-ray diffraction experiment was conducted on a PANalytical X′Pert Pro diffractometer using Cu target Kα radiation at

ambient temperature.To investigate the internal strucetures of the buttons, a JEM 2010 transmission electron microscope(TEM) was used and for the TEM study, thin foils were prepared by using a precision ion miller (Gatan 691). The transformation temperatures of Ni-Ti-Fe-Si subjected to homogenization annealing were determined by using a DSC 204 F1 Phoenix differential scanning calorimeter (NETZSCH, Germany) in the temperature range from -150℃ to 150℃ at the cooling and heating rates of 10K/min. The mechanical properties were measured by carrying out the room-temperature compression tests on an INSTRON-5500R testing machine at a constant strain rate of 10^{-3} s^{-1}. The specimens for compression tests, with a gauge dimension of φ4mm×6 mm, were carefully cut from the as-homogenized buttons.

3 RESULTS AND DISCUSSION

The XRD patterns of the $Ti_{51.8}Ni_{(45-x)}Fe_{3.2}Si_x$ alloys with different Si contents have been shown in Fig.1, in which the diffraction peaks corresponding to B2 austenite phase as well as the binary intermetallics Ti_2Ni can be seen and no obvious peaks corresponding to B19′ can be observed. Thus, it can be perceived that the alloys are entirely austenite at room temperature.

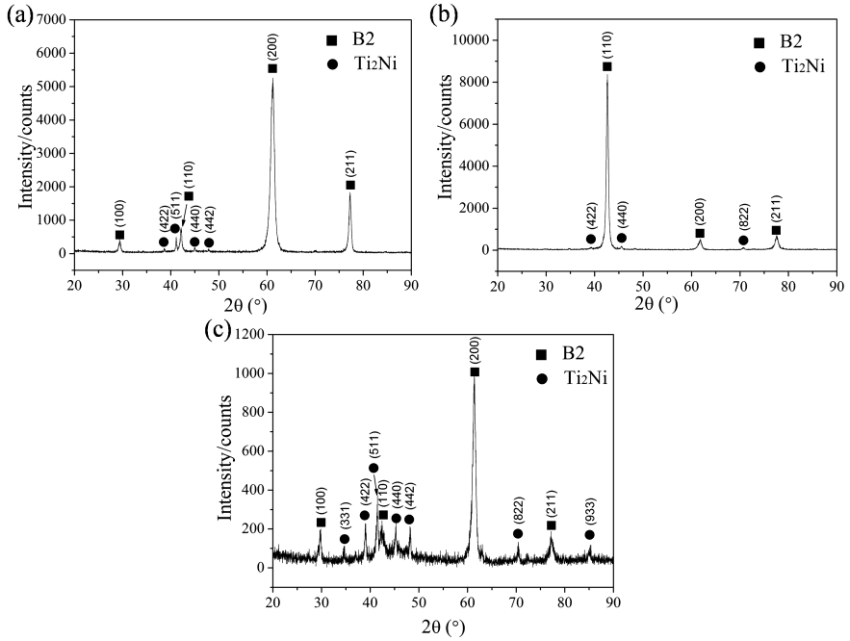

Figure 1: XRD patterns of three kinds of $Ti_{51.8}Ni_{(45-x)}Fe_{3.2}Si_x$ alloys: (a) x=0.3; (b) x=0.6; (c) x=0.9.

The SEM micrographs of the TiNiFeSi alloys and the chemical compositions of corresponding areas marked in micrographs are given in Fig.2-4. As can be seen in the micrographs, the alloys consist of amounts of irregular phases in a continuous matrix. According to the calibrated results of XRD, it's deduced that the dispersive phase is Ti_2Ni. Furthermore, the results of EDS analysis, shown in Fig.2-4 (b), indicate that the atomic ratios of Ni (31-34 at.pct) in particles are about half as much as the atomic ratios of Ti (62-64 at.pct). The EDS analysis results are further proof that the secondary phase is Ti_2Ni. Meanwhile, the EDS results in the matrix area is always in the range of 47.9 to 49.7 at.pct, as shown in Fig.2-4 (c). Thus, according to the NiTi phase diagram, a nonequilibrium peritectic reaction, $\beta+L\rightarrow\delta$ (Ti_2Ni), is expected to occur in the alloys during solidification, which results in Ti_2Ni phases forming as an external precipitate surrounding a Ti-rich metastable solid(Lopez, Salinas-Rodriguez, and

Rodriguez-Galicia 1996). Formation of Ti_2Ni can occur even in the equi-atomic NiTi alloys during solidification under certain conditions(Gupta, Mukherjee, and Johnson 1973). Furthermore according to the literature(Nagarajan and Chattopadhyay 1994), the addition of Si to Ni-Ti based alloys stabilizes icosahedral clusters and the clusters can subsequently serve as embryos for Ti_2Ni. As well as in the process of homogenization, the secondary phase Ti_2Ni precipitates on the crystal defects or at its boundaries(Lin, Wu, and Lin 1994). This can confirm that the composition of the second phase marked 1-3, is near to Ti_2Ni(Lopez, Salinas, and Calderon 2001; Moberly 1991). Seen from Fig.2-4 (a), the morphology and average size of the Ti_2Ni particles varies with the different contents of Si in TiNiFeSi alloys, of which $Ti_{51.8}Ni_{44.1}Fe_{3.2}Si_{0.9}$ has the largest particle size as well as regular particle morphology, and $Ti_{51.8}Ni_{44.4}Fe_{3.2}Si_{0.6}$, on the contrary, has the smallest particle size as well as anomalistic particle morphology. The morphology and average size of the Ti_2Ni particles in $Ti_{51.8}Ni_{44.7}Fe_{3.2}Si_{0.3}$ is somewhere in between. It is supposed that a little difference in the rapid nonequilibrium solidification results in the forming of Ti_2Ni with different shape and size. On the other hand, during annealing or quenching local fluctuation of the B2 matrix compositions leads to the precipitation of Ti_2Ni platelets in its immediate surroundings(Delville and Schryvers 2010). As a brittle intermetallic compound, Ti2Ni particles with different shape and size have influence on the phase transformation properties and mechanical properties.

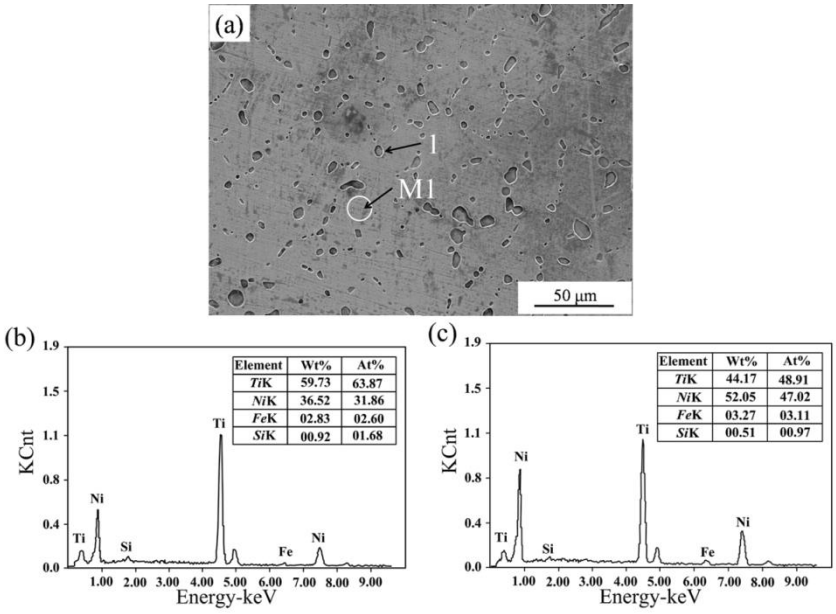

Figure 2: (a) The SEM micrograph of $Ti_{51.8}Ni_{44.7}Fe_{3.2}Si_{0.3}$ alloy after homogenizing treatment, and the composition analysis on area (b) 1, (c) M1 (marked in (a)), obtained from EDS measurements.

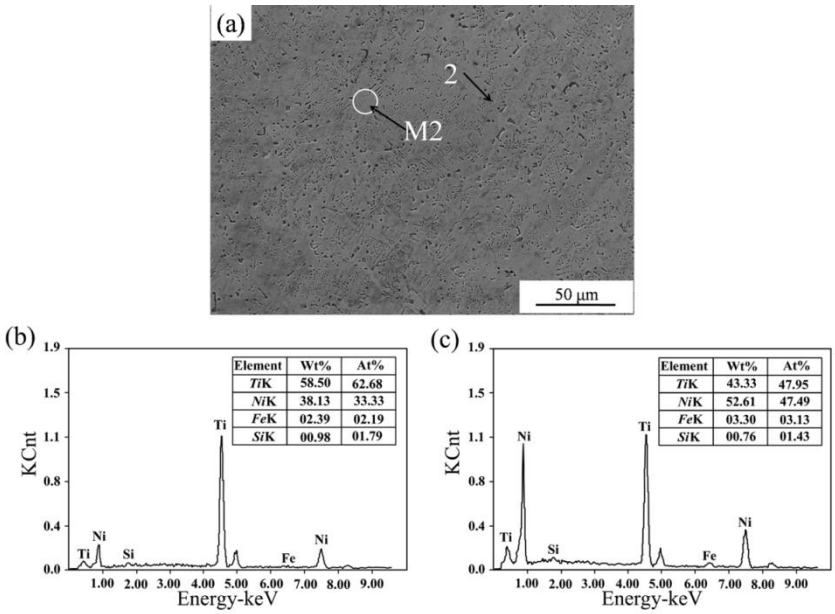

Figure 3: The SEM micrograph of $Ti_{51.8}Ni_{44.4}Fe_{3.2}Si_{0.6}$ alloy after homogenizing treatment, and the composition analysis on area (b) 2, (c) M2 (marked in (a)), obtained from EDS measurements.

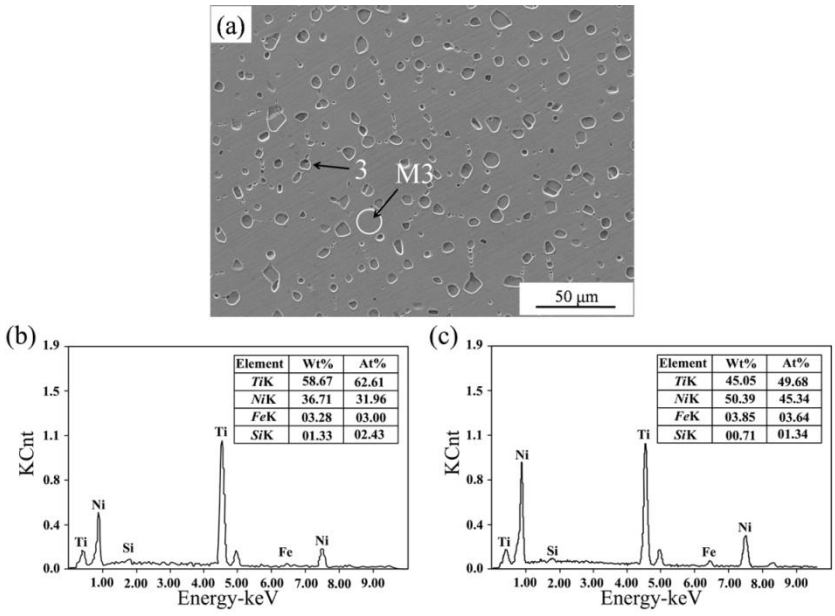

Figure 4: The SEM micrograph of $Ti_{51.8}Ni_{44.1}Fe_{3.2}Si_{0.9}$ alloy after homogenizing treatment, and the composition analysis on area (b) 3, (c) M3 (marked in (a)), obtained from EDS measurements.

The atomic proportions of Si in the alloys TiNiFeSi designed in this study are not high enough(less than 1 at.pct) to change the microstructure. Thus, $Ti_{51.8}Ni_{44.7}Fe_{3.2}Si_{0.3}$ samples were chosen as a representative of TiNiFeSi alloys series to conduct TEM experiments. Fig.5 (a) and (b) show the TEM bright field(BF) image of the matrix and the corresponding selected area diffraction pattern(SADP) taken along the zone axis [001], respectively, of the homogenization-treated $Ti_{51.8}Ni_{44.7}Fe_{3.2}Si_{0.3}$ alloy designed in this study. With the help of SADP(Fig.4(b)), the alloy matrix shown in Fig.5 (a) proved to be B2 parent phase, identified with the XRD data. Fig.5 (c) shows the other region where an integrated Ti_2Ni precipitate, which has been proved by the corresponding SADP shown in Fig.5(d), with the size

larger than 1 μm is clearly distinguished from the surrounding matrix by obvious boundary. It can be seen that the analysis results of TEM further confirm the anterior results of XRD and EDS.

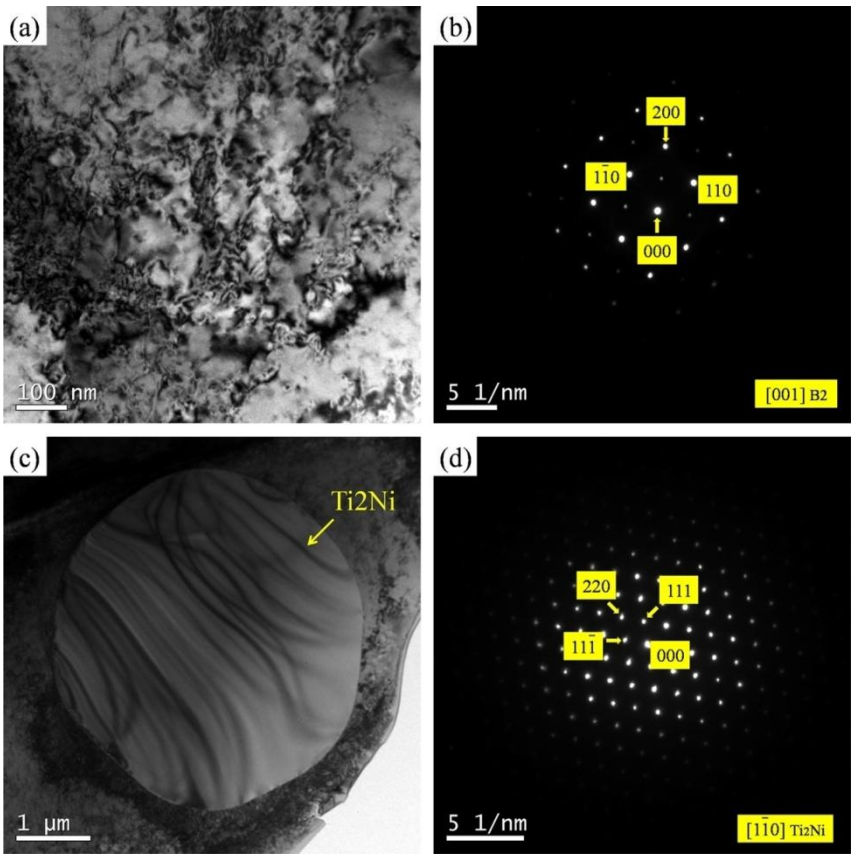

Figure 5: TEM observations of the as-homogenized $Ti_{51.8}Ni_{44.7}Fe_{3.2}Si_{0.3}$ alloys. (a) BF image of the B2 matrix. (b) SADP with a zone axis [001] taken from (a). (c) BF image of the coherent Ti2Ni precipitates in the B2 matrix. (d) SADP with a zone axis [1-10] taken from (c).

3.1 Phase transformation behavior

It has been said that the two-stage transformation of austenite (B2)→R-phase (R)→martensite (B19′) occurs in the Ti-Ni alloys that include traces of a third element such as Fe and Al(Marquina et al. 1994; Matsumoto and Honma 1976; Hara et al. 1997). The DSC experimental results for $Ti_{51.8}Ni_{(45-x)}Fe_{3.2}Si_x$(x=0.3, 0.6, 0.9) are shown in Fig.6, from which it is seen that the DSC curves styles of the alloys in this work are almost same. As shown in Fig.6, Ti-Ni-Fe-Si alloys exhibit two-stage phase transformations during heating. Correspondingly, the first DSC peak accounts for the reverse transition B19′→R (denoted with Rp) and the second DSC peak corresponds to the reverse transition R→B2 (denoted with Ap) and, hence, the phase transformation sequence can be described as B19′→R→B2. However, only one exothermic peak appears during cooling part of the DSC cycle and it's deduced that the exothermic peak corresponds to the forward transition B2→B19′ (denoted with Mp) rather than the transition B2→R. In order to confirm that the exothermic peak means martensitic transformations rather than R-phase alone, the $Ti_{51.8}Ni_{44.7}Fe_{3.2}Si_{0.3}$ alloy was chosen to conduct the DSC experiment with an opposite temperature procedure. As can be seen by comparing Fig.6(a) and Fig.6(d), both are the results of DSC measurements for $Ti_{51.8}Ni_{44.7}Fe_{3.2}Si_{0.3}$, and have the familiar DSC curve forms. Fig.4(d) shows that the R-phase and austenitic transformations occurs again when the temperature rose from -150℃ to 150℃, so it can be decided that the specimen was in a state of

martensite at 150 degrees below zero, and, hence, the single exothermic peak during cooling corresponds to martensitic transformation.

In order to explore the rule of phase transformation, the temperature of Rp, Ap and Mp are carefully analyzed and the values are listed in Table 1. The transformation temperature of NiTiFeSi alloys is all below zero and the lowest phase transformation temperature is about minus 90 Celsius, on account of the addition of Fe (more than 3 at.pct). The results show that phase transformation peak temperature of the alloys is different from each other, and the peak temperature of $Ti_{51.8}Ni_{44.4}Fe_{3.2}Si_{0.6}$ is higher than the other two alloys. By comparison, $Ti_{51.8}Ni_{44.1}Fe_{3.2}Si_{0.9}$ has the lowest transformation peak temperature, and the phase transformation peak temperature of $Ti_{51.8}Ni_{44.7}Fe_{3.2}Si_{0.3}$ is in the middle. The phase transformation temperature is closely correlated with the microstructural of alloys shown in Fig.2-4(a). These brittle and hard Ti_2Ni particles can act as preferential sites for the development of local inner strain when the alloys are subjected to thermal processing, because size and elastic moduli mismatches between matrix and precipitates. Therefore, the coherent Ti_2Ni particles surrounded by strain fields, in turn, provide preferential sites for martensite nucleation and act as effective obstacles for the propagation of martensite interfaces(Nagarajan and Chattopadhyay 1994). In addition, the Ti_2Ni particles can maintain a fair extent of good relationship across the interface with the matrix, which can help in nucleation of martensite(Bhagyaraj et al. 2013). Since the alloy $Ti_{51.8}Ni_{44.4}Fe_{3.2}Si_{0.6}$ owns the smallest Ti_2Ni particle size and maximum particle number per unit area and can provide more nucleation sites, the Mp temperature of $Ti_{51.8}Ni_{44.4}Fe_{3.2}Si_{0.6}$ is higher than the other two alloys. Whereas, during the heat part of DSC curve the Rp and Ap temperature of $Ti_{51.8}Ni_{44.4}Fe_{3.2}Si_{0.6}$ is higher than the other two alloys, which means the transformation of B19′→R→B2 is suppressed to some extent. It's concluded that the strain fields developed around large volume fractions of Ti_2Ni particles are considered to suppress the formation of of R-phase and austensite which accompanies with lattice deformation in the matrix of martensite.

Table 1：Results of DSC measurement of the alloys

Temperature	Rp (℃)	Ap (℃)	Mp (℃)
$Ti_{51.8}Ni_{44.7}Fe_{3.2}Si_{0.3}$	-80.5	-11.7	-19.9
$Ti_{51.8}Ni_{44.4}Fe_{3.2}Si_{0.6}$	-73.9	-5.8	-13.0
$Ti_{51.8}Ni_{44.1}Fe_{3.2}Si_{0.9}$	-88.1	-16.1	-24.6

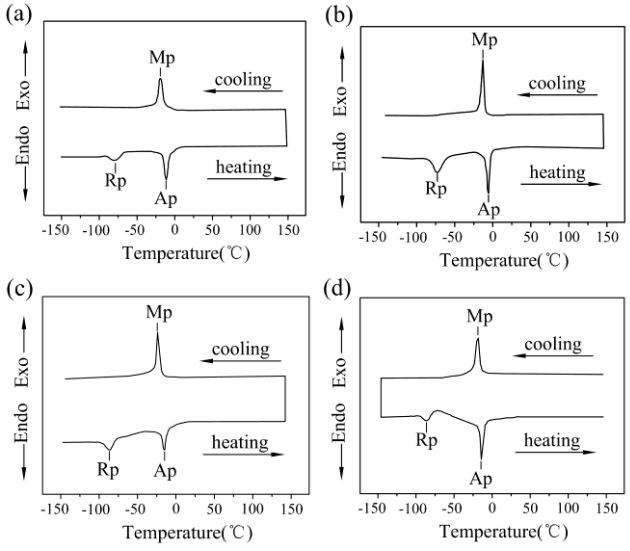

Figure 6: DSC heating-cooling curves for $Ti_{51.8}Ni_{(45-x)}Fe_{3.2}Si_x$ alloys: (a) x=0.3; (b) x=0.6; (c) x=0.9 and (d) cooling-heating curves of $Ti_{51.8}Ni_{44.7}Fe_{3.2}Si_{0.3}$. Mp, peak temperature of the B2→B19′ transformation; Rp, peak temperature of the B19′→R transformation; Ap, peak temperature of the R→B2 transformation.

3.2 Mechanical properties

The mechanical behaviors of $Ti_{51.8}Ni_{(45-x)}Fe_{3.2}Si_x$ alloys in austenite state were tested at room temperature, as shown in Fig.7. All the alloys exhibit one-stage yielding in the stress-strain curve, which represents that the deformation temperature exceeds the maximal critical mechanically induced martensitic transformation temperature. It is found that the yield strength and rupture strength of $Ti_{51.8}Ni_{44.1}Fe_{3.2}Si_{0.9}$ is higher than that of $Ti_{51.8}Ni_{44.7}Fe_{3.2}Si_{0.3}$ and $Ti_{51.8}Ni_{44.4}Fe_{3.2}Si_{0.6}$ has the lowest yield strength and highest rupture strength. It's obviously that the mechanical behaviors of $Ti_{51.8}Ni_{(45-x)}Fe_{3.2}Si_x$ alloys has close relations with the morphology and average size of the Ti_2Ni particles. The increase in the critical stress for slip deformation of $Ti_{51.8}Ni_{(45-x)}Fe_{3.2}Si_x$ alloys can be attributed to the coherent Ti_2Ni(Nam et al. 2008). The Ti_2Ni precipitates in the $Ti_{51.8}Ni_{44.1}Fe_{3.2}Si_{0.9}$ has the largest particle size as well as regular particle morphology, which notably increases the yield strength and rupture strength of the alloys. However, the rupture strength of $Ti_{51.8}Ni_{44.4}Fe_{3.2}Si_{0.6}$ is abnormally higher than the other two alloys, and it's concluded that the micro-sized Ti2Ni particle could disturb or impede the crack growth and increase the rupture strength of the alloys. All the alloys in this study exhibit excellent plasticity. For $Ti_{51.8}Ni_{44.4}Fe_{3.2}Si_{0.6}$ alloy with the best plasticity in the three alloys, the reduction in height can reach 50%.

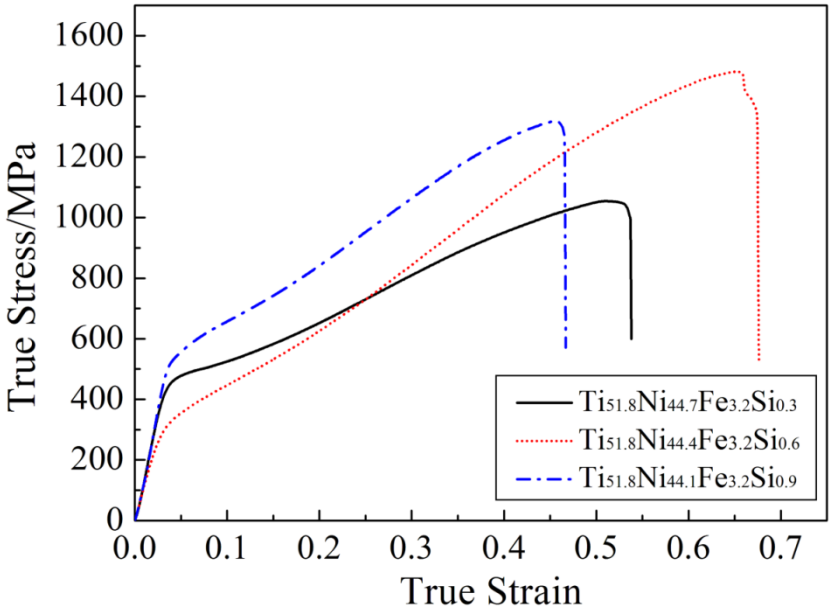

Figure 7: Compressive stress-strain curves of $Ti_{51.8}Ni_{(45-x)}Fe_{3.2}Si_x$ alloys

4 Conclusions

(1) The composition $Ti_{51.8}Ni_{(45-x)}Fe_{3.2}Si_x$ (x=0.3, 0.6, 0.9；at.%) processed in this study is effective in generating Ti_2Ni phase. The component and phase analysis were studied using EDS and XRD. All three Ni-Ti-Fe-Si SMAs consist of B2 austenite and Ti_2Ni precipitates. The microstructures of three

kinds of Ni-Ti-Fe-Si SMAs were studied using SEM and TEM. The microstructures are characterized by various morphology and size of the Ti_2Ni phase. The contents of Si play an important role in changing the morphology and size of Ti_2Ni phase in the three Ni-Ti-Fe-Si alloys.

(2) The phase transformation was studied using DSC. The Ti-Ni-Fe-Si SMAs exhibit two-stage phase transformations during heating and one-stage phase transformation during cooling part of DSC cycle, which can be attributed to the influence of amounts of Ti_2Ni precipitates. Furthermore, the morphology and size of Ti_2Ni phase could affect the phase-transition temperature slightly.

(3) The small and dispersed Ti_2Ni particles in $Ti_{51.8}Ni_{44.4}Fe_{3.2}Si_{0.6}$ can significantly improve the rupture strength of the alloys, but the yield strength is reduced to about 300MPa. When the size and morphology of Ti_2Ni is not much different from each other, the yield and rupture strength of $Ti_{51.8}Ni_{44.1}Fe_{3.2}Si_{0.9}$, in which Ti2Ni particles are larger and more uniform, is higher than that of $Ti_{51.8}Ni_{44.7}Fe_{3.2}Si_{0.3}$.

Reference

Basu, Ritwik, Jain, Lokendra, Maji, Bikas, and Krishnan, Madangopal. 2015. Dynamic recrystallization in a Ni–Ti–Fe shape memory alloy: Effects on austenite–martensite phase transformation. *Journal of Alloys and Compounds*, **639**: 94-101.

Bhagyaraj, J., Ramaiah, K. V., Saikrishna, C. N., Bhaumik, S. K., and Gouthama. 2013. Behavior and effect of Ti2Ni phase during processing of NiTi shape memory alloy wire from cast ingot. *Journal of Alloys and Compounds*, **581**: 344-51.

Delville, Rémi, and Schryvers, Dominique. 2010. Transmission electron microscopy study of combined precipitation of Ti2Ni(Pd) and Ti2Pd(Ni) in a Ti50Ni30Pd20 alloy. *Intermetallics*, **18** (12): 2353-60.

Gallagher, PCJ. 1970. The influence of alloying, temperature, and related effects on the stacking fault energy. *Metallurgical Transactions*, **1** (9): 2429-61.

Gao, F., and Wang, H. M. 2008. Effect of TiNi in dry sliding wear of laser melt deposited Ti2Ni/TiNi alloys. *Materials Characterization*, **59** (9): 1349-54.

Gupta, SP, Mukherjee, K, and Johnson, AA. 1973. Diffusion controlled solid state transformation in the near-equiatomic Ti-Ni alloys. *Materials Science and Engineering*, **11** (5): 283-97.

Hara, Toru, Ohba, Takuya, Okunishi, Eiji, and Otsuka, Kazuhiro. 1997. Structural study of R-phase in Ti-50.23 at.% Ni and Ti-47.75 at.% Ni-1.50 at.% Fe alloys. *Materials Transactions, JIM*, **38** (1): 11-7.

Kim, Yeonwook, and Jang, Seungkyu. 2013. Martensitic transformation behaviors of Ti-rich Ti–Ni alloy fibers fabricated by melt overflow. *Materials Research Bulletin*, **48** (12): 5045-8.

Lin, H.C., Wu, S.K., and Lin, J.C. 1994. The martensitic transformation in Ti-rich TiNi shape memory alloys. *Materials Chemistry and Physics*, **37** (2): 184-90.

Lopez, H, Salinas-Rodriguez, A, and Rodriguez-Galicia, J. 1996. Microstructural aspects of precipitation and martensitic transformation in a Ti-rich Ni-Ti alloy. *Scripta Materialia*, **34** (4): 659-64.

Lopez, H, Salinas, A, and Calderon, H. 2001. Plastic straining effects on the microstructure of a Ti-rich NiTi shape memory alloy. *Metallurgical and Materials Transactions A*, **32** (3): 717-29.

Marquina, M, Jimenez, M, Marquina, V, Aburto, S, Ridaura, R, Gómez, R, Escudero, R, and Ríos-Jara, D. 1994. Structural transitions in a TiNiFe shape memory alloy. *Materials Characterization*, **32** (3): 189-93.

Matsumoto, M, and Honma, T. 1976. Martensitic Transformation of Intermetallic Compound Ti 50 Ni 47 Fe 3. *New Aspects of Martensitic Transformation. Japan Institute of Metals, Tokyo. 1976, 199-204*.

Mehrabi, K., Bahmanpour, H., Shokuhfar, A., and Kneissl, A. 2008. Influence of chemical composition and manufacturing conditions on properties of NiTi shape memory alloys. *Materials Science and Engineering: A*, **481-482**: 693-6.

Moberly, Warren John. 1991. *Mechanical twinning and twinless martensite in ternary Ti50Ni (50-x) Mx intermetallics*.

Nagarajan, R, and Chattopadhyay, K. 1994. Intermetallic Ti2Ni/TiNi nanocomposite by rapid solidification. *Acta Metallurgica et Materialia*, **42** (3): 947-58.

Nam, TaeHyun, Lee, JaeHwa, Nam, JungMin, Kim, KiWon, Cho, GyuBong, and Kim, YeonWook. 2008. Microstructures and mechanical properties of Ti–45at.%Ni–5at.%Cu alloy ribbons containing Ti2Ni particles. *Materials Science and Engineering: A*, **483-484**: 460-3.

Qian, Yanping, Liu, FuShun, Li, Yan, and Xu, Huibin. 2006. Influence of Rolling Deformation on the Structural and Mechanical Properties of TiNiFe Shape Memory Alloys. *ACTA AERONAUTICA ET ASTRONAUTICA SINICA-SERIES A AND B-*, **27** (2): 336.

Salamon, M. B., Meichle, M. E., and Wayman, C. M. 1985. Premartensitic phases ofTi50Ni47Fe3. *Physical Review B*, **31** (11): 7306-15.

Sato, AKIKAZU, Chishima, E, Yamaji, Y, and Mori, T. 1984. Orientation and composition dependencies of shape memory effect in Fe-Mn-Si alloys. *Acta Metallurgica*, **32** (4): 539-47.

Wang, J. G., Liu, F. S., and Cao, J. M. 2010. The microstructure and thermomechanical behavior of Ti50Ni47Fe2.5Nd0.5 shape memory alloys. *Materials Science and Engineering: A*, **527** (23): 6200-4.

Wu, Lingmei, and Wu, Shyikaan. 2010. The evolution of Ti2Ni precipitates in annealed Ti51Ni49shape memory melt-spun ribbons. *Philosophical Magazine Letters*, **90** (4): 261-8.

Zhang, CS, Wang, YQ, Chai, W, and Zhao, LC. 1991. The study of constitutional phases in a Ni47Ti44Nb9 shape memory alloy. *Materials Chemistry and Physics*, **28** (1): 43-50.